

**Full title:**

Lipid and nucleocapsid N-protein accumulation in COVID-19 patient lung and infected cells

**Short title:**

SARS-CoV-2 infection induces lipid and N-protein accumulation

Anita E. Grootemaat<sup>1</sup>, Sanne van der Niet<sup>1</sup>, Edwin R. Scholl<sup>1</sup>, Eva Roos<sup>2</sup>, Bernadette Schurink<sup>2</sup>, Marianna Bugiani<sup>2</sup>, Sara E. Miller<sup>3</sup>, Per Larsen<sup>1,2</sup>, Jeannette Pankras<sup>1,2</sup>, Eric A. Reits<sup>1</sup>, Nicole N. van der Wel<sup>1\*</sup>

**Contact information**

<sup>1</sup>Electron Microscopy Centre Amsterdam, Medical Biology, Amsterdam University Medical Centre AMC, the Netherlands

<sup>2</sup>Department of Pathology, Amsterdam University Medical Centers (UMC), VU University Amsterdam, Amsterdam, the Netherlands

<sup>3</sup>Department of Pathology, Duke University Medical Center, Durham, NC, USA

\*Corresponding author: Nicole van der Wel

email address: n.n.vanderwel@amsterdamumc.nl

## Abstract

The pandemic of the severe acute respiratory syndrome coronavirus 2 (SARS-CoV-2) has caused a global outbreak and prompted an enormous research effort. Still, the subcellular localization of the corona virus in lungs of COVID-19 patients is not well understood. Here, the localization of the SARS-CoV-2 proteins is studied in postmortem lung material of COVID-19 patients and in SARS-CoV-2 infected Vero cells, processed identically. Correlative light and electron microscopy on semi-thick cryo-sections, demonstrated induction of electron-lucent, lipid filled compartments after SARS-CoV-2 infection in both lung and cell cultures. In infected Vero cells and using immuno-electron microscopy, viral proteins were detected in these lipid filled compartments. In addition, several viral proteins were detected in virus particles, Golgi, double membrane spherules and multiple-virus bodies which were not lysosomal. In lung tissue, the non-structural protein 4 and the stable nucleocapsid N-protein, were detected on membranes of lipid filled compartments. The induction of such lipid filled compartments and the localisation of the viral proteins in lung of patients with fatal COVID-19, may explain the extensive inflammatory response.

## Authors Summary

The trafficking of coronaviruses in lung of COVID-19 patients is not well understood and virus particles are difficult to find. Here we have visualized virus particles in SARS-CoV-2 infected cells by focusing on viral protein detection, in combination with ultrastructure. We studied how the virus is altering the cell morphology and determined that in Vero cells, lipid filled compartments contained various viral proteins. In these cells, also membrane enclosed multi-virus bodies were visible that contain a different set of viral proteins. We demonstrated that lipid filled compartments are viral induced compartments, as no known cellular marker such as lipid droplet or lysosomal marker was present. Using this knowledge, we then studied lung tissue from patients with a fatal SARS-Cov-2 infection, processed in a similar manner. Again we detected lipid filled compartments, now with viral

46 proteins nsp4 and the stable nucleocapsid N-protein. The presence of these lipid filled compartments  
47 with viral proteins induced by SARS-CoV-2 infections, could be why the immune response of the  
48 COVID-19 patients is so strong, resulting in a fatal infection, and should be considered for new  
49 therapeutic strategies.

50

# Introduction

The outbreak of Severe Acute Respiratory Syndrome Coronavirus 2 (SARS-CoV-2) in late 2019 is the third major outbreak of  $\beta$ -coronaviruses in the human population of the past two decennia, together with the smaller outbreaks of Severe Acute Respiratory Syndrome Coronavirus (SARS-CoV-1) in 2003 and Middle East Respiratory Syndrome coronavirus (MERS-CoV) in 2012.

SARS-CoV-2 belongs to the family *Coronaviridae*, a large family of single-stranded positive-sense RNA ((+)RNA) viruses. The first two-thirds of the genome typically codes for polyproteins that, once processed by proteases, produce non-structural proteins involved in viral replication [1]. The remaining third of the genome consists of four structural proteins: envelope (E), membrane (M), nucleocapsid (N), and spike (S). Coronaviruses are well known for their ability to induce high membrane plasticity in host cells, where the membrane rearrangements lead to the formation of viral replication organelles (ROs) [2–10]. As observed in SARS-CoV-1, MERS-CoV, and the closely related coronavirus murine hepatitis virus (MHV), the ROs consist of convoluted membranes (CMs) that are interconnected with double-membrane vesicles (DMVs) and appear to be continuous with the membranes that constitute the endoplasmic reticulum (ER) [2,11–17]. Elaborate studies using immuno-fluorescence and electron microscopy (EM) techniques demonstrate that DMVs contain double-stranded RNA (dsRNA) which can be used as a marker of (+)RNA virus replication [2,3,18,19]. Taken together, these findings indicate that the RO serves as the replication and transcription site in which the DMVs, may provide a zone safe from detection by the innate immune sensors and degradation by RNA degradation machinery in the host cell [20,21].

The formation of DMVs has been shown to be facilitated by coronaviral non-structural proteins (nsps) [22]. Co-expression of three virally encoded transmembrane proteins, namely nsp3, nsp4, and nsp6, has been found to be sufficient for the production of DMVs in SARS-CoV-1 and MERS-CoV where the interactions of nsp3 and nsp4 result in the pairing and curving of membranes, and nsp6 contributes to the production of vesicles [9,10,23]. A recent publication, using cryo-electron tomography (cryo-ET), shows DMVs of SARS-CoV-2 and MHV in a native host cellular environment containing pore

complexes that were not found in previous studies using conventional EM methods [18]. Additionally, the publications by Wolff *et al.* 2020 [24] and Klein *et al.* 2020 [17] demonstrate the presence of N-protein in these DMVs.

The subcellular localization of the viral proteins and virus particles is based on infections in cultured cells. In patient material, viral proteins have been localized at a cellular level in various organs of COVID-19 patients [25], including human kidney [26], and in lungs of cynomolgus macaques [27]. These studies used light microscopy to find regions of interest, and some of the studies subsequently used EM to find virus particles. One of the hurdles to overcome is the correct identification of viral particles in patient material such as lung [12,28–32], kidney [33–39] and other organs reviewed in [6]. Recent publications show data on the morphology and size of isolated SARS-CoV-2 particles [40–43] and virus particles in Vero E6 cells [17] with the use of conventional EM and cryo-EM, although this data alone is not always sufficient to recognize viral proteins or virus particles. Bullock *et al.* proposed a set of eight rules for the correct identification of coronaviruses [6]. Following these rules, a closer inspection of 27 articles where supposed SARS-CoV-2 particles in patient-derived samples have been found, revealed that according to Bullock and Miller, only four articles correctly identified virus [6,44–47]. The most common misinterpretations were clathrin-coated vesicles as single SARS-CoV-2 particles and endosome-derived multi-vesicular bodies (MVBs) as ROs [6,47].

To assist in this identification conundrum, labelling of antibodies directed against specific viral proteins can be of use. In this article, we provide the first insights into the localizations of both structural and non-structural proteins in SARS-CoV-2-infected Vero cells and compare this with identically processed patient samples retrieved during the first wave of SARS-CoV-2 infections using immuno-gold labelling and CLEM.

# **Results**

## **Immuno-Electron Microscopy on SARS-CoV-2-infected Vero**

### **Cells**

Since the outbreak of COVID-19, the identification of virus particles using EM in lung has been a heavily debated subject [6,48,49]. Based on the morphology, it is, especially in postmortem material, difficult to discriminate single virus particles from clathrin-coated vesicles, and MVBs have been interpreted as clusters of virus particles. Therefore, we decided to employ immuno-gold labelling, which can be used to decorate (viral) proteins specifically with 10- or 15-nm gold particles to distinguish them from cell organelles. This way, virus particles with M-, N-, or S-protein and the replication complexes with non-structural proteins can be identified by the gold attached to the specific antibodies. To validate whether the antibodies used for recognition of the proteins in FM [50] can be used on patient materials fixed with an extended fixation protocol, we first tested these antibodies on SARS-CoV-2-infected Vero cells. The antibodies were used on uninfected and 24-hour infected Vero cells fixed for 1, 3, and 14 days as we have fixed patient material in a similar manner. Different antibodies against viral proteins were tested (see Materials and Methods), and successful labelling and their subcellular localizations are described.

### **Characterization of virus particles with N-protein**

Immuno-gold labelling of SARS-CoV-1 structural proteins using a mouse anti-SARS-CoV-1-N (46-4) antibody demonstrated that the nucleocapsid protein (N-protein or N) is detected in the cytosol and on virus particles in several subcellular structures (Figs 1, S1) of infected cells. The N-protein can be specifically detected, as no labelling was detected on uninfected cells. Therefore, all membrane enclosed spherical structures ranging in size from 60 to 120 nm in diameter and with an electron-dense core (e-dense, black) [6,41], are annotated here as virus particles. Note that in cells and tissues stained with osmium and embedded in resin, membranes appear e-dense, whereas using the immuno-EM

method on cryo-sections, membranes appear electron-lucent (e-lucent, white) [51]. This is due to the fact that with the immuno-EM method, membranes are not stained, but only surrounding proteins in the cytosol are stained with uranyl acetate. In 24-hour infected Vero cells, small clusters of N-protein can be detected in proximity to double membrane structures, bending around the N-protein cluster similar to that in the cryo-EM sections (Fig S1), [18]. Coronaviruses are known to be a membrane enveloped viruses, mostly detected inside host membrane structures [6,52], and indeed the majority of the virus particles are surrounded by membranes. Intact viruses are identified close to the Golgi (Fig S2), inside multi-virus bodies (MViB) (Fig S3), inside open e-lucent structures (Fig S4), and in the core of double membrane spherules (DMS) [3,17] (Figs 1A, 1B). In DMSs, virus particles are spherical, but in the other compartments, both spherical and oval shaped virus particles are visible. The size of the virus particles are measured inside MViBs, DMS and intracytoplasmic and are categorized as spherical or oval-shaped. All particles are measured at the longest axis of N-protein-positive particles that have a clear membrane and e-dense core present. The average size between the spherical and oval-shaped virus is slightly different, but not statistically significant. Inside MViBs, spherical particles are  $87 \text{ nm} \pm 17 \text{ nm}$  versus  $109 \pm 26 \text{ nm}$  for the oval-shaped particles (Table 1). Also, no difference in size is measured at different subcellular locations. Different EM techniques result in slightly different sizes, being  $97 \pm 12 \text{ nm}$  for oval-shaped cryo-EM fixed extracellular SARS-CoV-2 [43] or  $99 \text{ nm}$  in resin-embedded spherical virus [41]. Thus, in 24-hour infected Vero cells N-protein-positive virus particles can be detected as spherical 87-nm or 109-nm oval-shaped membrane structures with an e-dense core, present close to Golgi, in DMS, or in multi-vesicular structures.

## **Classification of virus-containing compartments**

As the presence of SARS-CoV-2 in multi-vesicular structures in lung is heavily debated [6,48], we studied the presence of lysosomal markers like CD63 in the multi-virus bodies (Fig S3). The Vero cell line is a kidney epithelial cell line from African green monkey, but antibodies against human CD63, a glycosylated transmembrane protein containing a putative lysosomal-targeting/internalisation motif, can be detected in multi-lamellar bodies (MLB) which are lysosomal compartments. Only some CD63 label is detected in the multi-vesicular bodies (Fig S3F). Therefore, we propose that the compartments

in which the viral N-protein is detected, is not a true lysosome, but rather a multi-virus body. More elaborate studies on different stages of infection and blocking lysosomal acidification combined with immuno-EM have to be performed to determine the role of these MViBs during viral replication.

CD63 is also detected on early endosomes but not present on the majority of the e-lucent structures detected in clusters in SARS-CoV-2 infected cells (Fig S4). These structures seem to be induced by the virus infection, as uninfected cells contain larger lipid droplets but not the clustered e-lucent structures of 327 nm +/- 130 nm. High magnification analyses reveal that the e-lucent compartments appear to be filled with lipid like structures (Figs 1, S4F, S4H), much like we previously described for *Mycobacterium tuberculosis* infected cells [53]. Therefore, Nile red staining was performed on both uninfected and SARS-CoV-2 infected Vero cells, and a clear increase in Nile red signal is observed in infected cells (Fig 2). Indeed, others already demonstrated that lipid accumulation occurs after SARS-CoV-2 infection in Vero cells [54,55]. To prove that the e-lucent compartments detected with EM are Nile red positive and thus lipid-containing compartments, both FM and EM were performed on the same section and combined in a CLEM image (Fig 2C). These CLEM images demonstrate that at least a part of the e-lucent compartments are lipid filled. The structure of these compartments is not identical to lipid droplets (LD), so we used an antibody specific for perilipin-2, which is known to localize in LD [56] to determine if the SARS-CoV-2 induced lipid filled compartments are in fact lipid droplets. Immuno-gold labelling is present on typical LD in uninfected Vero cells but not on the lipid filled compartments detected in SARS-CoV-2 infected cells (Figs 2F and 2G). Based on the absence of both the lysosomal marker CD63 and LD marker perilipin-2, these e-lucent structures are not lysosomes, nor LD but rather novel lipid-filled compartments induced by SARS-CoV-2 infection.

### **Localisation of M-protein and non-structural proteins nsp4 and nsp13**

The localisation of different viral proteins in cultured cells can be used to understand the pathology and replication of SARS-CoV-2 in lung tissue of COVID-19 patients. In infected Vero cells, the same procedures as for N-protein were applied to detect nsp3, but immuno-gold label is very limited, and thus, we conclude that this antibody does still recognize its substrate after 14 days of glutaraldehyde-



paraformaldehyde fixation (Table 2). The non-structural proteins nsp4 and nsp13 are detected on vesicles located nearby and attached to the Golgi stacks (Fig S2). The signal of nsp13 is limited to a few gold particles per Golgi stack, and nsp4 is more distinct, but also has some background on mitochondria (Fig S4G). The M-protein abundantly labels Golgi stacks and vesicles around the Golgi. Interestingly, nsp4, nsp13, and M are also detected on MVIBs (Fig S3) and at e-lucent lipid filled compartments, while uninfected cells are unlabelled (Figs 1, S4). These structures resemble double membrane vesicles (DMVs) or single membrane vesicles described for MHV, SARS-CoV-1, SARS-CoV-2, and MERS-CoV infected cells [3,5,16–18,23,50]. Single-membrane vesicles are proposed to be derived from the ER-to-Golgi intermediate compartment [57], and play a role in the secretion of virus to be released into extracellular space. With immuno-EM labelling only on some cellular compartments, a double membrane is detected (Fig S4H, blue arrows), which could be explained by the EM-technique used. Rather than performing high pressure fixation and freeze substitution [3] or cryo-EM [17,18], we used conventional fixation to be able to compare Vero cells with lung tissues of COVID-19 patients. It is possible that the double membranes are lost during fixation for immuno-EM, as Snijder et al already demonstrated in 2006 [16]. Another limitation of the immuno-EM is that no clear spike proteins are detected on extracellular virus particles (Fig 3), though conventional sample preparation using osmium staining and embedding does show spikes [11,41] as does cryo-EM [17,18]. Extracellular virus particles are immuno-labelled for both N- and M-protein. Interestingly, the majority of the extracellular virus particles are not spherical, but rather oval-shaped. The subcellular localisation of N-, M-protein and nsps in infected Vero cells is summarized in Table 2, and translation of this knowledge to patient material could be essential for understanding COVID-19 pathogenesis in patients. As immuno-localisation with the antibodies against N-, M-protein, and nsp4, are specific and survive glutaraldehyde fixation, these antibodies can be used for analysis of lung tissues.

## **Immuno-EM on lung of COVID-19 patients**

In lung of COVID-19 patients, we searched for the presence of virus and replication organelles using antibodies selected on infected Vero cells. Material of 7 COVID-19 patients from a prospective

autopsy cohort study performed at Amsterdam University Medical Centers (UMC) [25] were included. With informed consent from relatives, full body autopsies were performed, and lung material was fixed for EM analysis. Materials were fixed for 1, 3 or 14 days. From those 7 patients, the lung tissues of 2 were too damaged to use for EM due to a postmortem delay. From our previous light microscopy analysis [25], we learned that only in a part of the lung tissue of a COVID-19 patient N-protein can be detected, and virus particles are difficult to find. Thus, in order to find the infected region of interest (ROI), we first performed fluorescence microscopy on sections of tissues processed for EM, so that when we identified a ROI containing viral proteins, EM could be performed (approached as in van Leeuwen et al., 2018). Semi-thick 0,3- $\mu$ m slices were incubated with antibodies against SARS-CoV-1 nsp3, nsp4, nsp13, and structural proteins N-, M-, and S-protein. We focused on areas near small blood vessels and alveolar walls, as our previous LM analysis revealed infected cells present along the alveolar walls. These cells were identified to be pneumocytes, stromal cells in the septa, endothelial cells in the septal capillaries, and alveolar macrophages [25]. Fluorescence microscopy showed that the N-protein (Fig 4) and nsp4 (Fig 5) could be detected. Noteworthy is the higher background for the M antibody and the relatively low labelling for nsp3 and nsp13 (Table 3).

Thus, in lung tissue from COVID-19 patients, an ROI was selected by FM using the N-protein antibody. In one patient (patient 64), relatively large clusters of N-protein were detected (Fig 4A) often in a perinuclear region. As in Vero cells (Fig 2), an increase in lipid accumulation, was observed (Figs 4B, 4C). Nile red staining was combined with N-protein labelling, and N-protein and lipid accumulations, localize in the same general areas but did not co-localize at the same subcellular localisation. Control lung material processed identically to COVID-19 patient material and tested for lipid accumulation demonstrated homogeneous background staining. Sections of 150 nm were analysed with both FM and EM and combined (Fig 4D). In line with our CLEM data on the Vero cells, performing CLEM on lung tissue demonstrated that lung tissue also accumulates lipid in e-lucent compartments. Then ultrathin 60-nm cryo-sections were cut, and protein A conjugated to 10-nm gold particles was used to label N-protein.

The ultrastructure of the lung tissue is reasonable, given the fact that this is postmortem material and that it is from a patient with COVID-19. The tissue is unlike healthy lung tissue, not ventilated, but instead filled with erythrocytes and packed with inflammatory cells infiltrating the alveolar lumen and inter-alveolar septa. It is not always possible to identify the cell type specially when the nucleus is not present in the 60-nm thin section. N-protein is detected in cells with large e-lucent compartments, with some label found in e-lucent, lipid filled compartments. Only a few spherical single membrane structures with N-protein were detected, but these can be cytosolic, and, unlike in Vero cells, surrounded by membrane (Fig 4 inset). These might be virus-like particles, but due to the low labelling (1 gold particle), the on average larger diameter (110 nm), and an atypical localisation in the cytosol, over-interpretation is possible. Nonetheless, large clusters of viruses are not detected. Besides the limited labelling on small round vesicles, N-protein is also present on membranous structures close to e-lucent compartments (Figs 4F, S5). These structures are not present in all patients; from the 7 patients investigated, 2 had clusters of proteins detectable with the SARS-CoV-1 anti N-protein. In patient 64 (patient description in Schurink et al., 2020), relatively large N-protein clusters at the e-lucent compartments were detected (Figs 4F, S5A-D), and smaller clusters are detected in patient 58, albeit at a similar location [on membrane clusters near the e-lucent compartments (Figs S5E, S5F)].

Using FM, nsp4 was identified in the same ROI of lung tissue used for detection of N-protein (Fig 5). Cells positive for nsp4 are present in various tissue compartments. Although background labelling is detected, some cells are brightly positive. Immuno-EM demonstrates nsp4 on e-lucent compartments, which appear filled with lipid like structures. A small amount of label is detected on mitochondria which should be regarded as background labelling, as this is also present on uninfected Vero cells (Fig S4G). The summary of subcellular viral protein localisation in lung is presented in Table 3 and, compared to the quantity of labelling in Vero cells, less labelling is detected in only limited compartments. The lipid filled compartments, however, are positive for nsp4, and N-protein is accumulated close to these compartments. Like in Vero cells, lysosomal marker CD63 is absent from these compartments and thus the lipid filled compartments in lung are non-lysosomal. To our

knowledge, these lipid filled compartments, containing viral proteins nsp4 and N-protein, have not been identified before and need to be further characterized.

## Discussion

Since the outbreak commenced, the identification of corona viruses in lung by EM has been debated, and several articles had to be revised [47,59,60]. Experienced Electron Microscopists [6] have summarized these studies and suggest using one of 3 strategies: 1) visualisation of viral morphogenesis, 2) immuno-EM or *in situ* hybridization, or 3) visualization of particles *in situ* in tissue combined with biochemical evidence of viral presence. We chose immuno-EM with gold labelling using already validated antibodies raised against SARS-CoV-1 [50]. Immuno-EM on Vero cells identified the monoclonal anti-SARS-CoV-1-N 46-4 to be the best for the detection of nucleocapsid N-protein. Virus particles were detected in the process of development as denoted by clusters of cytosolic N-protein surrounded by double membranes (Figs 1, S1). Spherical and/or oval virus particles are detected in MViBs, in DMSs, and in membrane clusters in the cell. The spherical virus particles in DMSs ( $91 \text{ nm} \pm 15 \text{ nm}$ ) are slightly bigger than those in MViBs ( $87 \pm 17 \text{ nm}$ ) or in other regions of the cell ( $80 \pm 15 \text{ nm}$ ). Also, the oval-shaped virus particles are larger ( $109 \pm 26 \text{ nm}$  in MViBs and  $112 \pm 30 \text{ nm}$  for intracytoplasmic) than the spherical ones albeit, these variances are not statistically different. It should be noted that in immuno-EM and at 24 hours of infection, 20 % of the virus particles are scored as oval. The functional difference between spherical versus oval-shaped virus particles still has to be discovered but others have demonstrated that the oval or ellipsoidal-shaped virus particles contain more complexes of RNA and N-protein [43].

In lung of patients who had a fatal COVID-19 infection, virus-like particles are rarely detected even though the N-protein is detected in close proximity of the viral induced lipid filled compartments. In Vero cells however, N-protein is detected inside virus particles. It is possible that the difference is caused by incomplete fixation of lung or that ultrastructure is deteriorated in postmortem material. The

overall ultrastructure of the tissue, however, is acceptable (Figs 4, 5), because the postmortem time before lung tissue was fixed within a few hours, during the first wave of COVID-19 infections in the Netherlands. Finally, it is important to note that the magnification of EM makes finding 90-nm sized virus particles in a tissue block of 1x1 mm<sup>2</sup>, extremely difficult. Still, some studies have detected an occasional cell filled with virus-like particles [44–47].

Double membrane vesicles (DMVs), have been described in several EM studies [2,3,5,15–18] but are not so obvious in our immuno-EM images; only a few double membranes were identified surrounding e-lucent compartments (Fig S4, blue arrows), possible due to fixation limitations, as shown before by Snijder *et al.*, 2006 [16]. As double membranes were not recognizable, DMVs were not annotated in this study, and thus, it remains unclear if the DMVs detected in other studies are lipid filled.

Interestingly, our CLEM data (Figs 2 and 4) demonstrated that only part of the e-lucent compartments are lipid-filled. This could be due to the fact that only a subclass of the compartments are lipid filled, or could have a technical explanation. Lipids are notoriously difficult to fix with glutaraldehyde and paraformaldehyde alone [61], and thus part of the compartments might have lost the lipid content.

High resolution EM studies on cryo-preserved cells suggest DMVs to be filled with viral RNA with LD lying next to the DMVs [18]. For other viruses, lipid accumulation has been shown to be involved in viral replication [62–69] and some studies have demonstrated lipid accumulations in SARS-CoV-2-infected Vero cells [54] and also in infected human pulmonary epithelial Calu-3 cells [13]. Nardacci *et al.*, 2021, demonstrated that lipid accumulation is specific for SARS-CoV-2 and not for SARS-CoV-1 in a comparative electron microscopy study and established an increase of LD in lungs from deceased COVID-19 patients. Based on our immuno-EM, we propose the SARS-CoV-2 infection-induced compartments are not LDs, as they are irregular in shape and thus have a different morphology than spherical LDs. Also, based on the visible membrane, but also by the presence of transmembrane proteins nsp4 and nsp13, the lipid-filled compartments are surrounded by a bilayer, while lipid droplets are surrounded by a monolayer of phospholipids, which are perilipin-2 positive. Taken together, SARS-CoV-2 infection induces novel lipid filled compartments, different from LD or endosomes but with viral proteins nsp4 and N-protein.

Another virus induced structure is the already well described convoluted membranes, which was detected in Vero cells (Fig. 1B) but not in lung. In addition, multi-virus bodies were specifically detected in Vero cells and not in lung (Figs 1, S3). The MViBs are different from lysosomal MVBs, based on the fact that the MViBs are not CD63 positive and based on the size, morphology and the M-, N-protein labelling inside the virus detected within the structures. In the lung of patients with fatal COVID-19, no MViBs were detected. Recent comparison of SARS-CoV-2 infected Vero cells versus lung organoids demonstrated that the subcellular trafficking in Vero cells might be different [70] which can explain the presence of MViB in Vero and absence of these organelle in lung. Also the infections stage could be an explanation as we have analysed postmortem material and thus the last stage of the disease.

Remarkably, N-protein and nsp4 are detected in lung of patients in the last stage of the disease. It seems unlikely that only these 2 proteins are still produced by active replication of the virus, as no viral proteins were detected on the Golgi, but both N-protein and nsp4 could be more stable proteins and thus not degraded. The gene encoding the N-protein is conserved and stable, and the N-protein itself is both highly immunogenic and highly expressed during infection [71]. Work on patients with a SARS-CoV-1 infection demonstrated elevated levels of IgG antibodies against N-protein [72] and showed that N-protein is an antigen for T-cell responses, inducing SARS-CoV-1-specific T-cell proliferation and cytotoxic activity [73–75]. Also, in an increasing number of case studies, anti-N IgGs were detected in patients with severe COVID-19 [76] and in children, 5 out of 6 produced neutralizing IgG and IgM antibodies targeted to the N- and S-proteins of SARS-CoV-2 [77]. Interestingly, recent reports show that immune responses to the N-protein have been associated to poor clinical outcomes [78] and correlates with severity of COVID-19 [79].

In the current study, we detected N-protein in fatal COVID-19 infections using mouse anti-SARS-CoV-1-N 46-4 antibody, which recognizes an epitope located in the region between amino acids 50 to 200 [80], which is likely the RNA binding domain. A cryo-EM study demonstrated that the C-terminal region of the N-protein, is recognized and decorated by antibodies, and thus, is a potential immunogenic interaction site [81]. Further investigations of the stability of the various nsps and

structural proteins of SARS-CoV-2 might explain the observed differences in localisation in lung. Still, our electron microscopy studies showed the stable presence of N-protein and nsp4 and the induction of lipid filled compartments. Also for other viruses, like the dengue virus, accumulation of capsid on LD has been described, and, interestingly, inhibition of LD formation affected dengue virus replication [64]. Already, Dias demonstrated pharmacological inhibition via a key enzyme for LD formation effected SARS-CoV2 replication cells [52] suggestion that lipid accumulation is a potential drug target.

In conclusion, even after a fatal COVID-19 infection, virus particles are difficult to detect in lung, but immuno-EM demonstrated that in Vero cells SARS-CoV-2 virus particles are 90-nm spherical and 110-nm oval particles. Non-structural proteins nsp4 and 13 were detected in electron lucent, partly lipid-filled compartments that are induced upon infection with SARS-CoV-2 in Vero cells. In lung tissues, similar lipid-filled compartments are detected which are the sites of N-protein and nsp4 accumulation. We speculate that lipid-filled viral protein-containing compartments play an important role in the secondary effects of the disease. The uncontrolled immune responses causing the devastating damage of COVID-19 might be responding to either the proteins or even lipids accumulating in these novel subcellular compartments and thus provide new therapeutic strategies.

## Materials and Methods

### EM Infection and fixation of Cultured Vero Cells

Vero E6 were seeded ( $2.5 \times 10^6$  cells/T75 flask) one day before infection in MEM/25mM HEPES/2% fetal calf serum with penicillin and streptomycin. Cells ( $\sim 5 \times 10^6$  cells/T75) were infected with MOI=0.2 by adding the virus (nCoV-2019/Melb-1, ( $4.3 \times 10^6$  pfu/ml) to each T75 flask. Incubation was performed at 37°C for 24 hours. Then cells with and, as a control without virus, were fixed in 1 part medium plus 1 part 6% PFA + 0,4% GA in 0,4M PHEM buffer (240mM Pipes, 100mM HEPES, 8mM  $MgCl_2$  and 40mM EGTA at pH 6.9). After 1, 3 and 14 days of fixation samples were transferred to storage buffer (0,2M PHEM with 0,5% PFA).



361

## 362 **Collection and initial fixation of tissue from COVID-19 patients**

363 Autopsies were performed at Amsterdam University Medical Centers (UMC), at the VU Medical  
364 Center, and the Academic Medical Center, the Netherlands, according to the declaration of Helsinki.  
365 For this EM study, 7 patients with clinically confirmed COVID-19 for whom autopsy was requested,  
366 were included (Table 4). Ethical approval was granted by the institutional review board of Amsterdam  
367 UMC (METC 2020.167). As described by Schurink et al., 2020 COVID-19 was confirmed by  
368 quantitative real-time RT-PCR, and informed consent was obtained from the decedents' next of kin.  
369 During autopsy, lungs for conventional EM were fixed in Karnovsky fixative with 4% PFA with 1%  
370 GA in 0.1 M sodium cacodylate buffer. To avoid safety problems, samples were fixed for 14 days and  
371 transferred to storage buffer or embedded in gelatin and snap frozen.

## 372 **Embedding and sectioning**

373 After fixation, cells and tissue were washed 3 times with phosphate buffered saline (PBS) + 0.02M  
374 glycine (Merck, K27662101) to remove fixative. Cells were pelleted by centrifugation at 980 xg for 3  
375 minutes. Supernatant was removed, and cells were directly embedded in 12% gelatin (Sigma, G2500-  
376 500G) in 0.1 M phosphate buffer and pelleted by centrifugation for 3 minutes at 10,950 xg and  
377 solidified on ice, and blocks of ~1 mm<sup>2</sup> were cut with a razor blade. Lung tissue was cut into blocks of  
378 1-2 mm<sup>2</sup> and imbedded in a gelatin series of 2%, 6%, and 12% gelatin in 0.1 M phosphate buffer.  
379 Blocks of cells or tissue were incubated overnight in 2.3M sucrose at 4°C (Merck, K17687153) in  
380 0.1M phosphate buffer. Then samples were snap frozen and stored in liquid nitrogen. Sectioning was  
381 performed using a diamond knife (Diatome cryo-immuno) on a Leica Ultracut UC6 cryo-  
382 ultramicrotome. Semi thin sections (150-300 nm) were made at -80°C, and ultrathin sections were  
383 made at -120°C. The sections were transferred to a formvar-coated copper grid, gold finder grid, or  
384 glass slide in a droplet of 1 part 2% methylcellulose (Sigma, M6385-250G) to 1 part 2.3M sucrose.  
385 Sections were stored at 4°C until labelling.



## **Immuno-fluorescence labelling**

Semi-thin cryo-sections were transferred to gold finder grids for EM or to glass slides for light microscopy (LM) and washed with PBS + 0.02M glycine. Then, for LM, semi-thin sections were incubated on primary antibody for 1 hour in PBS + 0.1% bovine serum albumin (Sigma, A4503-50G) and washed with PBS + 0.02M glycine. Thereafter, they were incubated with secondary antibody conjugated to Alexa 488 (Mol. Probes, A32731), and in the last 5 minutes, Nile red (Sigma, 72485) and Hoechst 33342 (Thermo Fisher, H3570) was added. After washing with PBS, a cover slip was mounted with Vectashield (Vector laboratories, H-1000). Glass slides were imaged using a Leica DM6 widefield microscope with a 100x oil objective. Images were analyzed using ImageJ FIJI.

## **Immuno-gold labelling**

For EM, ultrathin sections were picked up and placed on 150 mesh copper grids and incubated on 2% gelatin in 0.1M phosphate buffer for 30 minutes at 37°C. Then, at room temperature, grids were washed with PBS + 0.02M glycine and blocked with 1% BSA in PBS. Grids were incubated with primary antibody in 1% BSA in PBS for 45 minutes. Then, grids were washed with PBS + 0.02M glycine. When the primary antibody was an unlabeled mouse monoclonal antibody, a secondary antibody, raised against mouse serum was used as a bridge to enhance labelling, followed by incubation with protein A conjugated with colloidal gold. In this case, background blocking was done by 0.1% BSA in PBS + 0.02M glycine, followed by incubation on rabbit anti mouse antibody (Z0259, DAKO) for 20 minutes and washed with PBS + 0.02M glycine. Again, grids were incubated in blocking solution and subsequently with protein A conjugated to 10-nm gold (Utrecht University). After washing with PBS, grids were incubated with 1% glutaraldehyde in PBS to fix the antibody-gold complex and washed 10 times for 2 minutes each with water. To contrast the samples, grids were incubated with uranyl acetate in 2% methylcellulose for 5 minutes, and the excess liquid was blotted from the grids with filter paper. Grids were imaged using a FEI Tecnai 120kV transmission electron microscope with a Veleta or Xarosa camera (EMSIS). Images were analyzed using imageJ FIJI.

## Correlative light and electron microscopy

For CLEM, we used a method described earlier [58]. In short; grids were washed with PBS + 0.02M glycine and incubated for 1 hour with primary antibody and again washed with PBS + 0.02M glycine. Thereafter, grids were incubated with secondary antibody Alexa 488 and in the last 5 minutes Nile red (Sigma, 72485) and Hoechst 33342 (Thermo Fisher, H3570) were added. After washing in PBS, the grids were mounted in between a glass slide and a coverslip in a droplet of Vectashield. CLEM samples were imaged on a Leica DM6 widefield microscope using a 100x oil objective. Images were analyzed using LasX. After widefield imaging, the coverslip was removed from the glass slide by pipetting PBS in between the coverslip and the glass slide. Vectashield was removed by washing the grid with milliQ water at 37°C. Thereafter, the grids were contrasted and imaged as described above. The correlation was performed using ICY eC-CLEM software.

## List of materials:

REAGENT or RESOURCE	SOURCE	IDENTIFIER
<b>Antibodies</b>		
Rabbit polyclonal anti-Nsp3	kind gift from Snijder laboratory	Leiden University Medical Centre; [16]
Rabbit polyclonal anti-Nsp4	kind gift from Snijder laboratory	Leiden University Medical Centre; [78]
Rabbit polyclonal anti-Nsp13	kind gift from Snijder laboratory	Leiden University Medical Centre; [16]
Rabbit polyclonal anti-M	kind gift from Snijder laboratory	Leiden University Medical Centre; [16]
Rabbit polyclonal anti-N anti-SARS-CoV-1-N (46-4)	kind gift from Snijder laboratory	Leiden University Medical Centre; [80]
Rabbit polyclonal anti-N	Sino Biological Inc	Cat#40143-T62
Mouse monoclonal anti-CD63	Santa Cruz	Cat#MX 49.129.5;RRID11817
Mouse monoclonal anti-Perilipin-2	Progen	Cat#610102;RRID00300-05
Rabbit Bridging anti mouse	DAKO	Cat#Z0259;RRID20007985
Goat anti mouse alexa488	Life technologies	Car#A21242;RRID1345066
Goat anti rabbit alexa488	Mol. Probes, Invitrogen	Cat#A27034;RRID2031072
Protein A conjugated to 10-nm gold	Utrecht University	www.cmc-utrecht.nl
<b>Chemicals</b>		
Nile red	Sigma-Aldrich	72485

Hoechst 33342	Thermo Fisher	H3570
Phosphate buffered saline	Gibco	18912-014
Glycine	Merck	K27662101
Gelatin	Sigma-Aldrich	G2500-500G; CAS9000-70-8
Methylcellulose	Sigma-Aldrich	M6385-250G; CAS9004-67-5
Bovine Serum Albumin	Sigma-Aldrich	A4503-50G; CAS9048-46-8
Vectashield	Vector Laboratories	H-1000
Uranyl acetate	EMS	22400
Virus strains		
nCoV-2019/Melb-1	kind gift from Snijder laboratory	
Experimental Models: Cell Lines		
Vero-cells	kind gift from Snijder laboratory	

## Acknowledgements

We like to thank Eric Snijder, Montse Barcena for input, discussion and providing SARS-CoV-2 infected Vero cells, Sabine Krom and Jordy de Bakker for technical assistance, Sandrine Florquin for providing control lung materials; ER, MB thank Funding Amsterdam UMC Corona Research Fund; SvdN was funded by NADP and NIH grant no. AI116604.

# References

1. Chen J, Malone B, Llewellyn E, Grasso M, Shelton PMM, Olinares PDB, et al. Structural Basis for Helicase-Polymerase Coupling in the SARS-CoV-2 Replication-Transcription Complex. *Cell*. Elsevier Inc.; 2020;182: 1560–1573.e13. doi:10.1016/j.cell.2020.07.033
2. Knoops K, Kikkert M, Van Den Worm SHE, Zevenhoven-Dobbe JC, Van Der Meer Y, Koster AJ, et al. SARS-coronavirus replication is supported by a reticulovesicular network of modified endoplasmic reticulum. *PLoS Biol*. 2008;6: 1957–1974. doi:10.1371/journal.pbio.0060226
3. Snijder EJ, Limpens RWAL, de Wilde AH, de Jong AWM, Zevenhoven-Dobbe JC, Maier HJ, et al. A unifying structural and functional model of the coronavirus replication organelle: Tracking down RNA synthesis. *bioRxiv*. 2020; doi:10.1101/2020.03.24.005298
4. Maier HJ, Hawes PC, Cottam EM, Mantell J, Verkade P, Monaghan P, et al. Infectious bronchitis virus generates spherules from zippered endoplasmic reticulum membranes. *MBio*. 2013;4: 1–12. doi:10.1128/mBio.00801-13
5. Ulasli M, Verheije MH, de Haan CAM, Reggiori F. Qualitative and quantitative ultrastructural analysis of the membrane rearrangements induced by coronavirus. *Cell Microbiol*. 2010;12: 844–861. doi:10.1111/j.1462-5822.2010.01437.x
6. Bullock HA, Goldsmith CS, Miller SE. Best practices for correctly identifying coronavirus by transmission electron microscopy. *Kidney Int*. Elsevier Inc; 2021;99: 824–827. doi:10.1016/j.kint.2021.01.004
7. Den Boon JA, Ahlquist P. Organelle-like membrane compartmentalization of positive-strand RNA virus replication factories. *Annu Rev Microbiol*. 2010;64: 241–256. doi:10.1146/annurev.micro.112408.134012
8. Romero-Brey I, Bartenschlager R. Endoplasmic reticulum: The favorite intracellular niche for

- viral replication and assembly. *Viruses*. 2016;8: 1–26. doi:10.3390/v8060160
9. Angelini MM, Akhlaghpour M, Neuman BW, Buchmeier MJ. Severe acute respiratory syndrome coronavirus nonstructural proteins 3, 4, and 6 induce double-membrane vesicles. *MBio*. 2013;4: 1–10. doi:10.1128/mBio.00524-13
10. Angelini MM, Neuman BW, Buchmeier MJ. Untangling membrane rearrangement in the nidovirales. *DNA Cell Biol*. 2014;33: 122–127. doi:10.1089/dna.2013.2304
11. Eymieux S, Rouillé Y, Terrier O, Seron K, Blanchard E, Rosa-Calatrava M, et al. Ultrastructural modifications induced by SARS-CoV-2 in Vero cells: a kinetic analysis of viral factory formation, viral particle morphogenesis and virion release. *Cell Mol Life Sci*. Springer International Publishing; 2021;78: 3565–3576. doi:10.1007/s00018-020-03745-y
12. Yao XH, He ZC, Li TY, Zhang HR, Wang Y, Mou H, et al. Pathological evidence for residual SARS-CoV-2 in pulmonary tissues of a ready-for-discharge patient. *Cell Res*. Springer US; 2020;30: 541–543. doi:10.1038/s41422-020-0318-5
13. Cortese M, Lee JY, Cerikan B, Neufeldt CJ, Oorschot VMJ, Köhrer S, et al. Integrative Imaging Reveals SARS-CoV-2-Induced Reshaping of Subcellular Morphologies. *Cell Host Microbe*. 2020;28: 853–866.e5. doi:10.1016/j.chom.2020.11.003
14. Hagemeijer MC, Ulasli M, Vonk AM, Reggiori F, Rottier PJM, de Haan CAM. Mobility and Interactions of Coronavirus Nonstructural Protein 4. *J Virol*. 2011;85: 4572–4577. doi:10.1128/jvi.00042-11
15. Mihelc EM, Baker SC, Lanman JK. Coronavirus infection induces progressive restructuring of the endoplasmic reticulum involving the formation and degradation of double membrane vesicles. *Virology*. Elsevier Inc.; 2021;556: 9–22. doi:10.1016/j.virol.2020.12.007
16. Snijder EJ, van der Meer Y, Zevenhoven-Dobbe J, Onderwater JJM, van der Meulen J, Koerten HK, et al. Ultrastructure and Origin of Membrane Vesicles Associated with the Severe Acute Respiratory Syndrome Coronavirus Replication Complex. *J Virol*. 2006;80: 5927–5940.

doi:10.1128/jvi.02501-05

17. Klein S, Cortese M, Winter SL, Wachsmuth-Melm M, Neufeldt CJ, Cerikan B, et al. SARS-CoV-2 structure and replication characterized by in situ cryo-electron tomography. *Nat Commun.* Springer US; 2020;11: 1–10. doi:10.1038/s41467-020-19619-7
18. Wolff G, Limpens RWAL, Zevenhoven-Dobbe JC, Laugks U, Zheng S, de Jong AWM, et al. A molecular pore spans the double membrane of the coronavirus replication organelle. *Science* (80- ). 2020;369: 1395–1398. doi:10.1126/SCIENCE.ABD3629
19. Gosert R, Kanjanahaluethai A, Egger D, Bienz K, Baker SC. RNA Replication of Mouse Hepatitis Virus Takes Place at Double-Membrane Vesicles. *J Virol.* 2002;76: 3697–3708. doi:10.1128/jvi.76.8.3697-3708.2002
20. Shulla A, Randall G. (+) RNA virus replication compartments: a safe home for (most) viral replication. *Curr Opin Microbiol.* 2016;32: 82–88.
21. Scutigliani EM, Kikkert M. Interaction of the innate immune system with positive-strand RNA virus replication organelles. *Cytokine Growth Factor Rev.* 2017;37: 17–27.
22. Siu YL, Teoh KT, Lo J, Chan CM, Kien F, Escriou N, et al. The M, E, and N Structural Proteins of the Severe Acute Respiratory Syndrome Coronavirus Are Required for Efficient Assembly, Trafficking, and Release of Virus-Like Particles. *J Virol.* 2008;82: 11318–11330. doi:10.1128/jvi.01052-08
23. Oudshoorn D, Rijs K, Limpens RWAL, Groen K, Koster AJ, Snijder EJ, et al. Expression and cleavage of middle east respiratory syndrome coronavirus nsp3-4 polypeptide induce the formation of double-membrane vesicles that mimic those associated with coronaviral RNA replication. *MBio.* 2017;8: 1–17. doi:10.1128/mBio.01658-17
24. Wolff G, Limpens RWAL, Zevenhoven-Dobbe JC, Laugks U, Zheng S, de Jong AWM, et al. A molecular pore spans the double membrane of the coronavirus replication organelle. *bioRxiv.* 2020;1398: 1395–1398. doi:10.1101/2020.06.25.171686

25. Schurink B, Roos E, Radonic T, Barbe E, Bouman CSC, de Boer HH, et al. Viral presence and immunopathology in patients with lethal COVID-19: a prospective autopsy cohort study. *The Lancet Microbe*. 2020;1: e290–e299. doi:10.1016/s2666-5247(20)30144-0
26. Ng JH, Bijol V, Sparks MA, Sise ME, Izzedine H, Jhaveri KD. Pathophysiology and Pathology of Acute Kidney Injury in Patients With COVID-19. *Adv Chronic Kidney Dis*. Elsevier Inc; 2020;27: 365–376. doi:10.1053/j.ackd.2020.09.003
27. Rockx B, Kuiken T, Herfst S, Bestebroer T, Lamers MM, de Meulder D, et al. Comparative pathogenesis of COVID-19, MERS and SARS in a non-human primate model. *Science* (80- ). 2020;368: 1012–1015. doi:10.1101/2020.03.17.995639
28. Pesaresi M, Pirani F, Tagliabracchi A, Valsecchi M, Procopio AD, Busardò FP, et al. SARS-CoV-2 identification in lungs, heart and kidney specimens by transmission and scanning electron microscopy. *Eur Rev Med Pharmacol Sci*. 2020;24: 5186–5188. doi:10.26355/eurev\_202005\_21217
29. Grimes Z, Bryce C, Sordillo EM, Gordon RE, Reidy J, Paniz Mondolfi AE, et al. Fatal Pulmonary Thromboembolism in SARS-CoV-2-Infection. *Cardiovasc Pathol*. 2020;48: 107227. doi:10.1016/j.carpath.2020.107227
30. Ackermann M, Verleden SE, Kuehnel M, Haverich A, Welte T, Laenger F, et al. Pulmonary Vascular Endothelialitis, Thrombosis, and Angiogenesis in Covid-19. *N Engl J Med*. 2020;383: 120–128. doi:10.1056/nejmoa2015432
31. Borczuk AC, Salvatore SP, Seshan S V., Patel SS, Bussel JB, Mostyka M, et al. COVID-19 pulmonary pathology: a multi-institutional autopsy cohort from Italy and New York City. *Mod Pathol*. Springer US; 2020;33: 2156–2168. doi:10.1038/s41379-020-00661-1
32. Bradley BT, Maioli H, Johnston R, Chaudhry I, Fink SL, Xu H, et al. Histopathology and ultrastructural findings of fatal COVID-19 infections in Washington State: a case series. *Lancet*. 2020;396: 320–332.

33. Su H, Yang M, Wan C, Yi LX, Tang F, Zhu HY, et al. Renal histopathological analysis of 26 postmortem findings of patients with COVID-19 in China. *Kidney*. 2020;98: 219–227.
34. Kissling S, Rotman S, Gerber C, Halfon M, Lamothe F, Comte D, et al. Collapsing glomerulopathy in a COVID-19 patient. *Kidney Int*. 2020;98: 228–231.  
doi:10.1016/j.kint.2020.04.006
35. Varga Z, Flammer AJ, Steiger P, Haberecker M, Andermatt R, Zinkernagel AS, et al. Endothelial cell infection and endotheliitis in COVID-19. *Lancet*. Elsevier Ltd; 2020;395: 1417–1418. doi:10.1016/S0140-6736(20)30937-5
36. Farkash EA, Wilson AM, Jentzen JM. Ultrastructural evidence for direct renal infection with sars-cov-2. *J Am Soc Nephrol*. 2020;31: 1683–1687. doi:10.1681/ASN.2020040432
37. Abbate M, Rottoli D, Gianatti A. Covid-19 attacks the kidney: Ultrastructural evidence for the presence of virus in the glomerular epithelium. *Nephron*. 2020; doi:10.1159/000508430
38. Menter T, Haslbauer JD, Nienhold R, Savic S, Hopfer H, Deigendesch N, et al. Postmortem examination of COVID-19 patients reveals diffuse alveolar damage with severe capillary congestion and variegated findings in lungs and other organs suggesting vascular dysfunction. *Histopathology*. 2020;77: 198–209. doi:10.1111/his.14134
39. Werion A, Belkhir L, Perrot M, Schmit G, Aydin S, Chen Z, et al. SARS-CoV-2 causes a specific dysfunction of the kidney proximal tubule. *Kidney Int*. 2020;98: 1296–1307.
40. Ke Z, Oton J, Qu K, Cortese M, Zila V, McKeane L, et al. Structures and distributions of SARS-CoV-2 spike proteins on intact virions. *Nature*. Springer US; 2020;588: 498–502.  
doi:10.1038/s41586-020-2665-2
41. Laue M, Kauter A, Hoffmann T, Möller L, Michel J, Nitsche A. Morphometry of SARS- CoV and SARS- CoV- 2 particles in ultrathin plastic sections of infected Vero cell cultures Michael. *Sci Rep*. 2021;11.



42. Turoňová B, Sikora M, Schürmann C, Hagen WJH, Welsch S, Blanc FEC, et al. In situ structural analysis of SARS-CoV-2 spike reveals flexibility mediated by three hinges. *bioRxiv*. 2020;208: 203–208. doi:10.1101/2020.06.26.173476
43. Yao H, Song Y, Chen Y, Wu N, Xu J, Sun C, et al. Molecular Architecture of the SARS-CoV-2 Virus. *Cell*. Elsevier Inc.; 2020;183: 730–738.e13. doi:10.1016/j.cell.2020.09.018
44. Martines RB, Ritter JM, Matkovic E, Gary J, Bollweg BC, Bullock H, et al. Pathology and pathogenesis of SARS-CoV-2 associated with fatal coronavirus disease, united states. *Emerg Infect Dis*. 2020;26: 2005–2015. doi:10.3201/eid2609.202095
45. Carsana L, Sonzogni A, Nasr A, Rossi RS, Pellegrinelli A, Zerbi P, et al. Pulmonary post-mortem findings in a series of COVID-19 cases from northern Italy: a two-centre descriptive study. *Lancet infect dis*. 2020;20: 1135–1140.
46. Falasca L, Nardacci R, Colombo D, Lalle E, DI Caro A, Nicastri E, et al. Postmortem Findings in Italian Patients with COVID-19: A Descriptive Full Autopsy Study of Cases with and without Comorbidities. *J Infect Dis*. 2020;222: 1807–1815. doi:10.1093/infdis/jiaa578
47. Dittmayer C, Meinhardt J, Radbruch H, Radke J, Heppner BI, Heppner FL, et al. Why misinterpretation of electron micrographs in SARS-CoV-2-infected tissue goes viral. *Lancet*. Elsevier Ltd; 2020;396: e64–e65. doi:10.1016/S0140-6736(20)32079-1
48. Goldsmith CS, Miller SE, Martines RB, Bullock HA, Zaki SR. Electron microscopy of SARS-CoV-2: a challenging task. *Lancet*. Elsevier Ltd; 2020;395: e99. doi:10.1016/S0140-6736(20)31188-0
49. Akilesh S, Nicosia RF, Alpers CE, Tretiakova M, Hsiang TY, Gale M, et al. Characterizing Viral Infection by Electron Microscopy: Lessons from the Coronavirus Disease 2019 Pandemic. *Am J Pathol*. American Society for Investigative Pathology; 2021;191: 222–227. doi:10.1016/j.ajpath.2020.11.003
50. Ogando NS, Dalebout TJ, Zevenhoven-Dobbe JC, Limpens RWAL, van der Meer Y, Caly L,

- et al. SARS-coronavirus-2 replication in Vero E6 cells: Replication kinetics, rapid adaptation and cytopathology. *J Gen Virol.* 2020;101: 925–940. doi:10.1099/jgv.0.001453
51. van der Wel NN, Hava D, Houben D, Fluitsma D, van Zon M, Pierson J, et al. M . tuberculosis and M . leprae Translocate from the Phagolysosome to the Cytosol in Myeloid Cells. *Cell.* 2007; 1287–1298. doi:10.1016/j.cell.2007.05.059
52. Bullock HA, Goldsmith CS, Zaki SR, Martines RB, Miller SE. Difficulties in differentiating coronaviruses from subcellular structures in human tissues by electron microscopy. *Emerg Infect Dis.* 2021;27: 1023–1031. doi:10.3201/eid2704.204337
53. Buter J, Cheng T-Y, Ghanem M, Grootemaat AE, Raman S, Feng X, et al. Mycobacterium tuberculosis releases an antacid that remodels phagosomes. *Nat Chem Biol.* Springer US; 2019;15: 889–899. doi:10.1038/s41589-019-0336-0
54. da Silva Gomes Dias S, Soares VC, Ferreira AC, Sacramento CQ, Fintelman-Rodrigues N, Temerozo JR, et al. Lipid droplets fuel SARS-CoV-2 replication and production of inflammatory mediators. *PLoS Pathog.* 2020;16: 1–19. doi:10.1371/journal.ppat.1009127
55. Nardacci R, Colavita F, Castilletti C, Lapa D, Matusali G, Meschi S, et al. Evidences for lipid involvement in SARS-CoV-2 cytopathogenesis. *Cell Death Dis.* Springer US; 2021;12. doi:10.1038/s41419-021-03527-9
56. Greenberg AS, Egan JJ, Wek SA, Garty NB, Blanchette-Mackie EJ, Londos C. Perilipin, a major hormonally regulated adipocyte-specific phosphoprotein associated with the periphery of lipid storage droplets. *J Biol Chem.* © 1991 ASBMB. Currently published by Elsevier Inc; originally published by American Society for Biochemistry and Molecular Biology.; 1991;266: 11341–11346. doi:10.1016/s0021-9258(18)99168-4
57. de Haan CAM, Rottier PJM. Molecular Interactions in the Assembly of Coronaviruses. *Adv Virus Res.* 2005;64: 165–230. doi:10.1016/S0065-3527(05)64006-7
58. van Leeuwen LM, Boot M, Kuijl C, Picavet DI, van Stempvoort G, van der Pol SMA, et al.

- 603           Mycobacteria employ two different mechanisms to cross the blood–brain barrier. *Cell*
- 604           *Microbiol.* 2018;20: 1–17. doi:10.1111/cmi.12858
- 605   59.   Dolhnikoff M, Ferreira Ferranti J, de Almeida Monteiro RA, Duarte-Neto AN, Soares Gomes-
- 606           Gouvêa M, Viu Degaspere N, et al. SARS-CoV-2 in cardiac tissue of a child with COVID-19-
- 607           related multisystem inflammatory syndrome. *Lancet Child Adolesc Heal.* 2020;4: 790–794.
- 608           doi:10.1016/S2352-4642(20)30257-1
- 609   60.   Kniss DA. Alternative interpretation to the findings reported in visualization of severe acute
- 610           respiratory syndrome coronavirus 2 invading the human placenta using electron microscopy.
- 611           *Am J Obstet Gynecol.* Elsevier Inc.; 2020;223: 785–786. doi:10.1016/j.ajog.2020.06.016
- 612   61.   Fujimoto T, Ohsaki Y, Suzuki M, Cheng J. Imaging Lipid Droplets by Electron Microscopy.
- 613           *Methods in Cell Biology.* 1st ed. Elsevier Inc.; 2013. pp. 227–251. doi:10.1016/B978-0-12-
- 614           408051-5.00012-7
- 615   62.   Villareal VA, Rodgers MA, Costello DA, Yang PL. Targeting host lipid synthesis and
- 616           metabolism to inhibit dengue and hepatitis C viruses. *Antiviral Res.* 2015;124: 110–121.
- 617           doi:10.1016/j.antiviral.2015.10.013.Targeting
- 618   63.   Lyn RK, Hope G, Sherratt AR, McLauchlan J, Pezacki JP. Bidirectional lipid droplet velocities
- 619           are controlled by differential binding strengths of HCV core DII protein. *PLoS One.* 2013;8.
- 620           doi:10.1371/journal.pone.0078065
- 621   64.   Filipe A, McLauchlan J. Hepatitis C virus and lipid droplets: Finding a niche. *Trends Mol Med.*
- 622           Elsevier Ltd; 2015;21: 34–42. doi:10.1016/j.molmed.2014.11.003
- 623   65.   Cheung W, Gill M, Esposito A, Kaminski CF, Courousse N, Chwetzoff S, et al. Rotaviruses
- 624           Associate with Cellular Lipid Droplet Components To Replicate in Viroplasms, and
- 625           Compounds Disrupting or Blocking Lipid Droplets Inhibit Viroplasm Formation and Viral
- 626           Replication. *J Virol.* 2010;84: 6782–6798. doi:10.1128/jvi.01757-09
- 627   66.   Coffey CM, Sheh A, Kim IS, Chandran K, Nibert ML, Parker JSL. Reovirus Outer Capsid

Protein  $\mu$ 1 Induces Apoptosis and Associates with Lipid Droplets, Endoplasmic Reticulum, and Mitochondria. *J Virol.* 2006;80: 8422–8438. doi:10.1128/jvi.02601-05

67. Samsa MM, Mondotte JA, Iglesias NG, Assunção-Miranda I, Barbosa-Lima G, Da Poian AT, et al. Dengue virus capsid protein usurps lipid droplets for viral particle formation. *PLoS Pathog.* 2009;5. doi:10.1371/journal.ppat.1000632

68. Ilnytska O, Santiana M, Hsu N, Du W, Chen Y, Viktorova EG, et al. Enteroviruses harness the cellular endocytic machinery to remodel the host cell cholesterol landscape for effective viral replication. *Cell Host Microbe.* 2013;14: 281–293. doi:10.1016/j.chom.2013.08.002. Enteroviruses

69. Melia CE, Peddie CJ, de Jong AWM, Snijder EJ, Collinson LM, Koster AJ, et al. Origins of enterovirus replication organelles established by whole-cell electron microscopy. *MBio.* 2019;10: 1–12. doi:10.1128/mBio.00951-19.

70. Beumer J, Geurts MH, Lamers MM, Puschhof J, Zhang J, Der J Van. A CRISPR / Cas9 genetically engineered organoid biobank reveals essential host factors for coronaviruses. *bioRxiv.* 2021;

71. Cong Y, Ulasli M, Schepers H, Mauthe M, V'kovski P, Kriegenburg F, et al. Nucleocapsid Protein Recruitment to Replication-Transcription Complexes Plays a Crucial Role in Coronaviral Life Cycle. *J Virol.* 2020;94: 1–21. doi:10.1128/jvi.01925-19

72. Leung DTM, Tam FCH, Chun HM, Chan PKS, Cheung JLK, Niu H, et al. Antibody response of patients with Severe Acute Respiratory Syndrome (SARS) targets the viral nucleocapsid. *J Infect Dis.* 2004;190: 379–386. doi:10.1086/422040

73. Dutta NK, Mazumdar K, Gordy JT. The Nucleocapsid Protein of SARS-CoV-2: a Target for Vaccine Development. *J Virol.* 2020;94: 1–2. doi:10.1128/jvi.00647-20

74. Shah VK, Fimal P, Alam A, Ganguly D, Chattopadhyay S. Overview of Immune Response During SARS-CoV-2 Infection: Lessons From the Past. *Front Immunol.* 2020;11: 1–17.

doi:10.3389/fimmu.2020.01949

75. Gao W, Tamin A, Soloff A, Aiuto LD, Nwanegbo E, Robbins PD, et al. Effects of a SARS-associated coronavirus vaccine in monkeys. *Lancet*. 2003;362: 1895–1896.
76. To KKW, Tsang OTY, Leung WS, Tam AR, Wu TC, Lung DC, et al. Temporal profiles of viral load in posterior oropharyngeal saliva samples and serum antibody responses during infection by SARS-CoV-2: an observational cohort study. *Lancet Infect Dis*. Elsevier Ltd; 2020;20: 565–574. doi:10.1016/S1473-3099(20)30196-1
77. Zhang Y, Xu J, Jia R, Yi C, Gu W, Liu P, et al. Protective humoral immunity in SARS-CoV-2 infected pediatric patients. *Cell Mol Immunol*. Springer US; 2020;17: 768–770. doi:10.1038/s41423-020-0438-3
78. Atyeo C, Fischinger S, Zohar T, Slein MD, Burke J, Loos C, et al. Distinct Early Serological Signatures Track with SARS-CoV-2 Survival. *Immunity*. Elsevier Inc.; 2020;53: 524–532.e4. doi:10.1016/j.immuni.2020.07.020
79. Shrock E, Fujimura E, Kula T, Timms RT, Lee IH, Leng Y, et al. Viral epitope profiling of COVID-19 patients reveals cross-reactivity and correlates of severity. *Science* (80- ). 2020;370. doi:10.1126/science.abd4250
80. Fang Y, Pekosz A, Haynes L, Nelson EA, Rowland RRR. Production and characterization of monoclonal antibodies against the nucleocapsid protein of SARS-CoV. *Adv Exp Med Biol*. 2006;581: 153–156. doi:10.1007/978-0-387-33012-9\_27
81. Casasanta MA, Jonaid GM, Kaylor L, Luqiu WY, Solares MJ, Schroen ML, et al. Microchip-based structure determination of low-molecular weight proteins using cryo-electron microscopy. *Nanoscale*. Royal Society of Chemistry; 2021;13: 7285–7293. doi:10.1039/d1nr00388g
82. Moriel-Carretero M. The hypothetical role of phosphatidic acid in subverting ER membranes during SARS-CoV infection. *Traffic*. 2020;21: 545–551. doi:10.1111/tra.12738

- 678 83. Van Hemert MJ, Van Den Worm SHE, Knoop K, Mommaas AM, Gorbelenya AE, Snijder EJ.  
679 SARS-coronavirus replication/transcription complexes are membrane-protected and need a  
680 host factor for activity in vitro. PLoS Pathog. 2008;4. doi:10.1371/journal.ppat.1000054  
681  
682

# Tables

Location	MViB		DMS	Intracytoplasmic	
Virus shape	spherical	oval	spherical	spherical	oval
x in nm	87±17	109±26	91±15	80±15	112±30
n	62	22	33	21	7

**Table 1. Average particle size at different subcellular locations.** Average size of virus particles in double membrane spherules (DMS), multi-virus bodies (MViB), and intracytoplasmic was measured and presented as average size (x) ± standard deviation and number of virus particles measured (n) in Vero cells infected with SARS-CoV-2 for 24 hours and immuno-gold labelled for N-protein with 10-nm gold.

Location in cell culture	N	M	Nsp3	Nsp4	Nsp13	CD63
Virus particle	+	+	-	-	-	-
Golgi	+/-	+	-	+	+/-	-
DMS	+	+/-	-	-	-	-
MViB	+	+	-	+/-	+/-	+/-
MLB	-	-	-	-	-	+
e-lucent compartment	+/-	+/-	-	+	+/-	-
extracellular virus particle	+	+	-	-	-	-

**Table 2. Immuno-gold labelling of viral proteins in SARS-CoV-2-infected Vero cells.** Presence of immuno-gold labelling on virus particles, Golgi, double membrane spherule (DMS), multi-virus bodies (MViB), multi-lamellar bodies (MLB), e-lucent compartments and extracellular virus particles in Vero cells infected with SARS-CoV-2 for 24 hours. Annotations: + present; - absent; +/- present but less prominent.

696

Location in lung	N	M	Nsp3	Nsp4	Nsp13	CD63
Virus particle	+/-	-	-	-	-	-
Golgi	-	-	-	-	-	-
DMS	-	-	-	-	-	-
MViB	-	-	-	-	-	-
MLB	-	-	-	-	-	+
e-lucent compartment	+/-	+/-	-	+	-	-
Extracellular virus particle	-	-	-	-	-	-

697 **Table 3. Immuno-gold labelling of viral proteins in SARS-CoV-2 infected lung.** Presence of  
698 immuno-gold labelling on virus particles, Golgi, double membrane spherule (DMS), multi-virus  
699 bodies (MViB), multi-lamellar bodies (MLB), e-lucent compartments and extracellular virus particles  
700 in patient 58 and 64 infected with SARS-CoV-2. Annotations: + present; - absent; +/- present but less  
701 prominent.

702

Patient	Infection stadium	Sex	Age	COV-N	Remarks
SVU 20-58	Limited infected cells in lung, limited systemic presence (HPB tract)	F	72	+	Data presented
SVU 20-39	Severe infected cells in lungs, systemic presence (GI tract)	M	73	+	
SVU 20-63	No presence in lung, limited presence in the heart	M	74	+	
SVU 20-64	Limited presence in the lung, no systemic presence	F	68	+	Data presented
SVU 20-155	-	F	75	+	
SVU 20-163	-	M	61	+	
SVU 20-174	-	M	78	+	
SVU 20-129	Control non-covid	M	68	-	
T18-5683	Control non-covid	F	5	-	Data presented
T18-10645	Control non-covid	F	15	-	



703 **Table 4. Patient description.** Information of patients from who autopsy material was taken with  
 704 informed consent and fixed for electron microscopy. In this study, electron micrographs were used  
 705 from patients SVU 20-58, SVU 20-64, and control T18-5683.

706

## Figure Legends

**Figure 1. Subcellular localisation of viral proteins in infected Vero-cells.** Vero cells were infected with SARS-CoV-2 for 24 hours and immuno-EM labelled with antibodies against SARS-CoV-1 proteins, followed by secondary antibodies conjugated to 10-nm gold particles. A) Clusters of N-protein labelling in cytosol (open arrows), and (enlarged in A') on double membrane spherules (right-most black arrow), or virus particles enclosed in a single membrane (two left-most black arrows). From the e-lucent compartment (red \*) a "virus-like" particle (as it is without N-protein labelling) is budding (white arrow). A'') enlarged area with MViB containing labelled and unlabelled virus-like particles. B) M-protein immuno-gold labelling on e-lucent compartments (gold is circled in red); in enlarged box, immuno-gold labelling on convoluted membrane structure (CM). Note virus-like particles are not labelled. C) Immuno-gold labelling of nsp4 on e-lucent compartments (circled in red) and various DMS without nsp4 labelling, also enlarged in C'. D) immuno-labelling of nsp13 on e-lucent compartments containing lipid like structures (red arrows). D') higher magnification of D. Immuno-gold decoration on e-lucent compartments is indicated by red circles; mitochondria by m, multiple virus body by MViB, convoluted membrane structure by CM, lipid like structures by red arrows, N-protein in cytosol by open arrows, N-protein labelled virus by black arrows, and black boxes indicate enlarged area.

**Figure 2. Lipid accumulates in e-lucent compartments more densely in infected Vero cells.** Fluorescence microscopy of DNA and lipid staining with Nile red in A) the uninfected control (Con) Vero cells and B) cells infected with SARS-CoV-2 for 24 hours; C) Electron microscopy of infected cells; D) Fluorescence microscopy of the same cells, and E) Correlative light-electron microscopy (CLEM) showing lipid staining at e-lucent compartments in the electron microscope. Immuno-EM labelling for lipid droplet marker perilipin-2 in F) uninfected Vero cells and G) cells infected with SARS-CoV-2 for 24 hours. Blue color in A, B, D, and E shows the nuclei stained with Hoechst and red shows the lipids stained with Nile red. In electron micrographs, lipid like structure is denoted by

red arrows, virus particles by black arrows, immuno-gold labelling of perilipin-2 by red circles, mitochondria by m, and lipid droplets by LD.

**Figure 3. Release of virus particles from Vero cells infected with SARS-CoV-2 for 24 hr. EM**

micrographs, demonstrate A) lack of immuno-gold labelling on extracellular virus particle using anti-nsp4, a non-structural protein of SARS-CoV-2 (black arrow); B) extracellular virus particles labelled with anti-N-protein, and C) anti-M-protein also labels on extracellular virus particles. Here, m represents mitochondrion, MViB multi-virus body.

**Figure 4. N-protein in e-lucent compartments in Lung COVID-19 patient. Lung from control and**

infected patients was either sectioned semi-thin for FM (A-C) or CLEM (D) and stained with Hoechst (blue) to identify nuclei, Nile red (red) to denote lipid, or anti-N-protein (green) to show N-protein, or it was ultrathin-sectioned for EM (E and F) and immuno-gold labelled using anti N-protein followed by secondary antibody tagged with 10-nm gold particles. A) COVID-19-infected lung showing accumulations of N-protein and Nile red stained lipids. B) overview of an uninfected control lung with no N-protein or lipid accumulation. C) Overview of infected lung with lipid accumulation. Identical section analysed by CLEM of infected lung demonstrate the e-lucent compartments present by EM (D) are Nile red and N-protein labelled (D') by the overlay of the FM on the EM micrograph (D'').

Immuno-gold labelling of infected lung with antibody against N-protein at low magnification (E) and magnified region from boxed area where lipid like structures (open red arrows) are visible (E') and a single virus particle with N labelling (E''), low magnification of N-protein labelling on membrane structures near the e-lucent compartments F); high magnification of F') clusters of N-protein labelling. Erythrocytes represented by e, nucleus by n, open red arrow lipid like structures, and boxed areas enlarged region.

**Figure 5. Non-structural protein 4 in e-lucent compartments infected lung. Lung tissue of**

COVID-19 patient 58 was either sectioned semi-thin for FM with A) nuclei, stained with Hoechst (blue), nsp4 stained with Alexa (green) in nsp4 positive cells indicated by white arrows and in black and white, and erythrocytes represented by e. Separate channels of nsp4 (B) and DNA (C). Ultrathin

758 sections of infected lung immuno-gold labelled against nsp-4 and 10-nm gold particles in overview  
759 (D) and at higher magnification (E) e-lucent compartments with nsp4 labelling on membrane and lipid  
760 like structures (open red arrows) erythrocytes represented by e. F) Schematic representation of  
761 uninfected Vero cells, SARS-CoV-2 infected Vero cells and lung tissue of COVID-19 patient  
762 summarizing presence cellular organelles and subcellular localisation viral proteins. In black: host  
763 compartments, in green: viral compartments, in red: lipid like structures, CM convoluted membrane  
764 DMS: double membrane spherules, G: Golgi, LD: lipid droplet, MLB: multi-lamellar bodies, MVIB:  
765 multi-virus body, LFC: lipid-filled compartment and immuno-labelling viral proteins: dark green  
766 triangle: nsp13, light green triangle: nsp4, blue circle: N-protein, yellow square: M-protein.



**Figure 1**

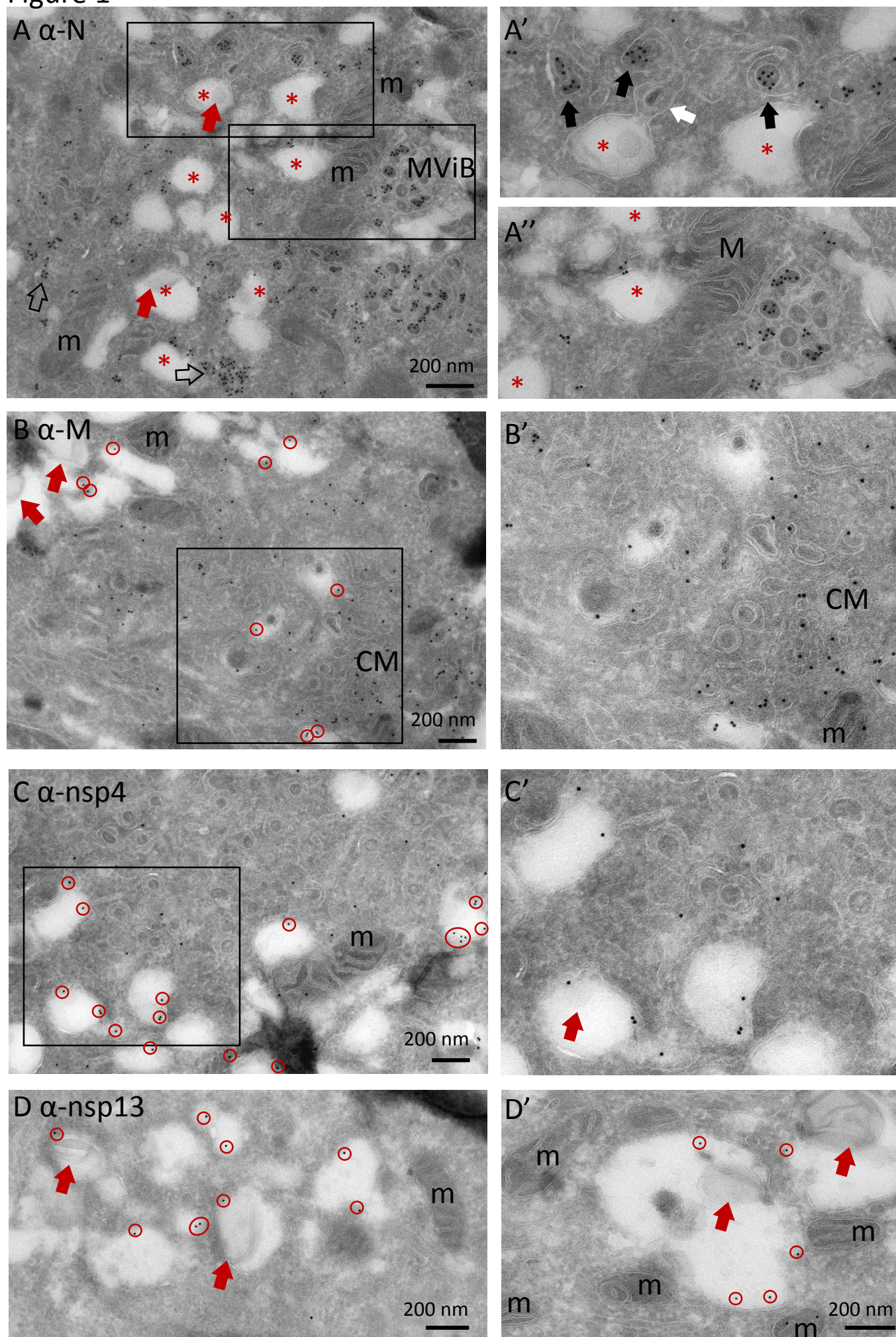
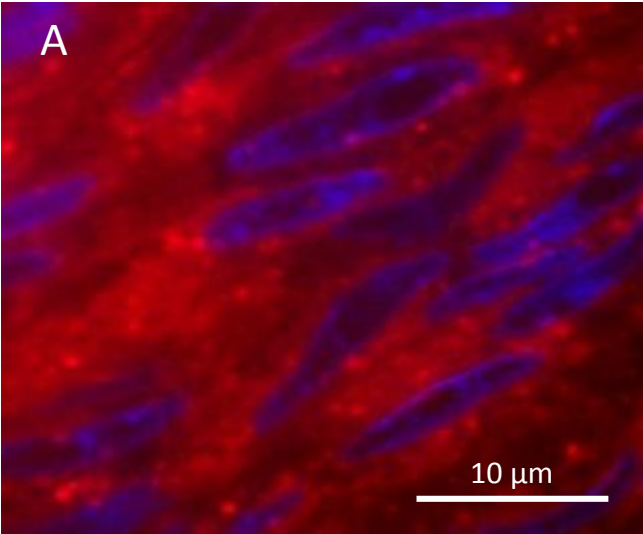


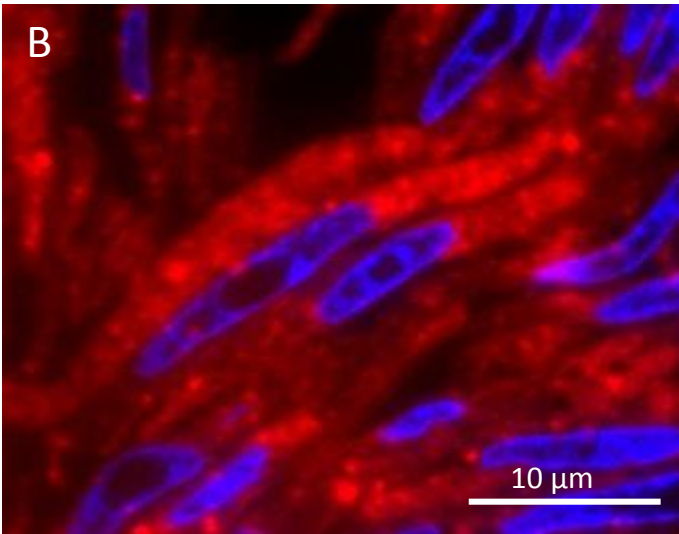


Figure 2

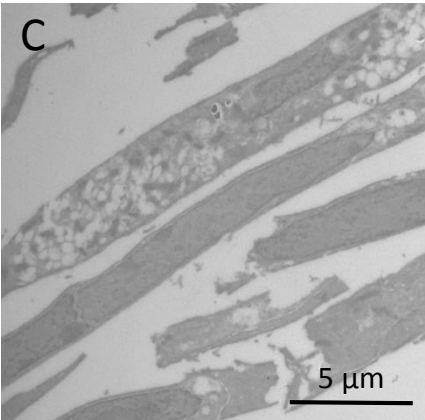
Con Vero: Lipid DNA



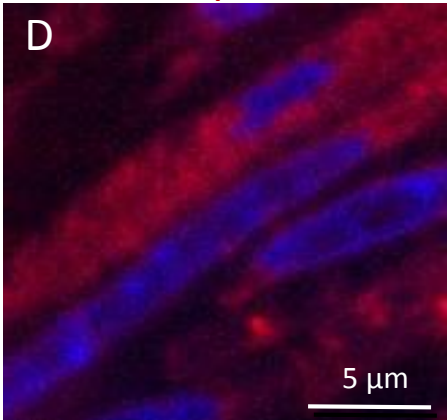
SARS-CoV-2 Vero: Lipid DNA



EM



FM: Lipid DNA



CLEM

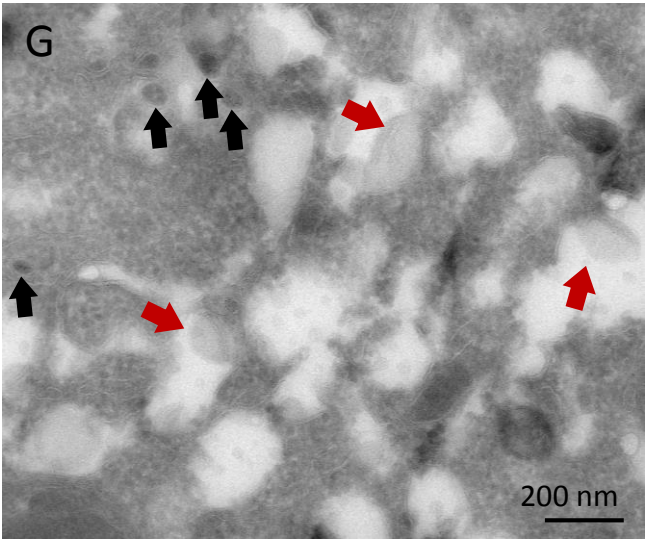
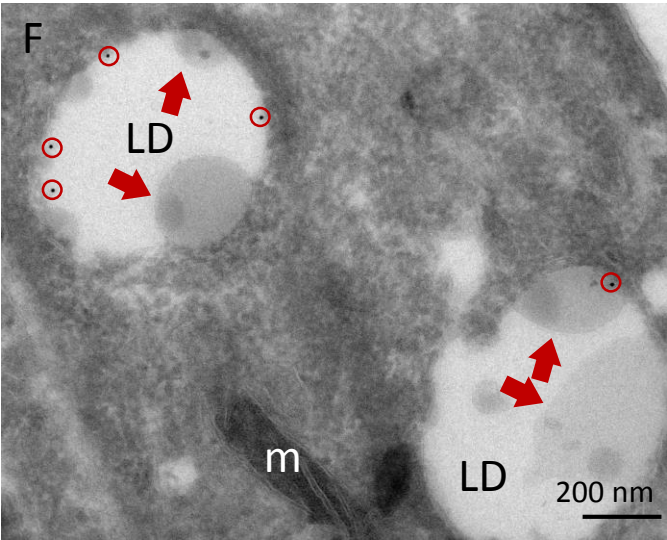
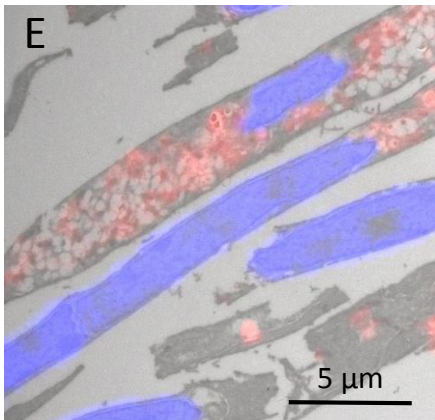


Figure 3

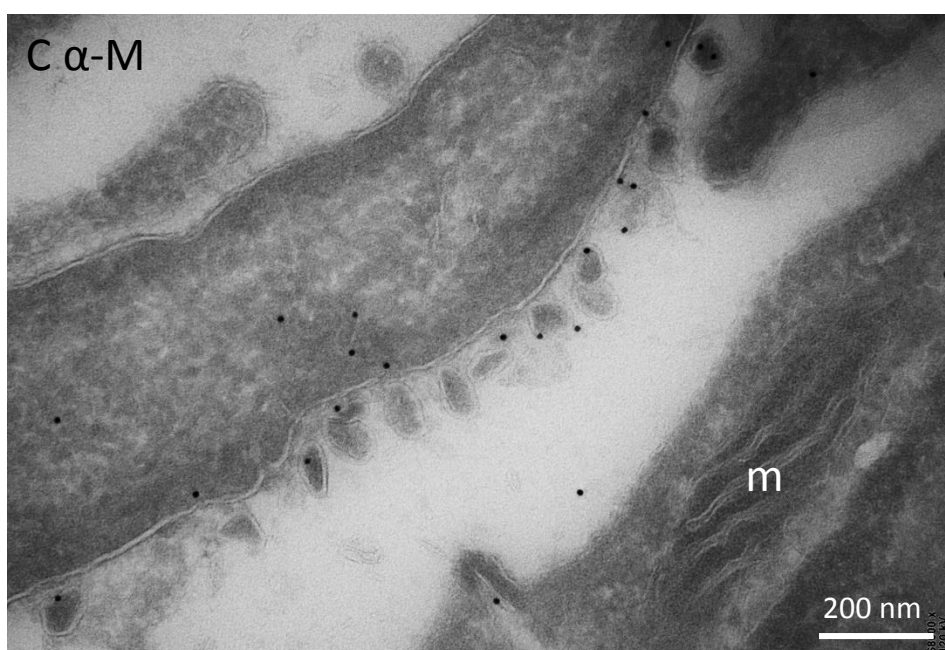
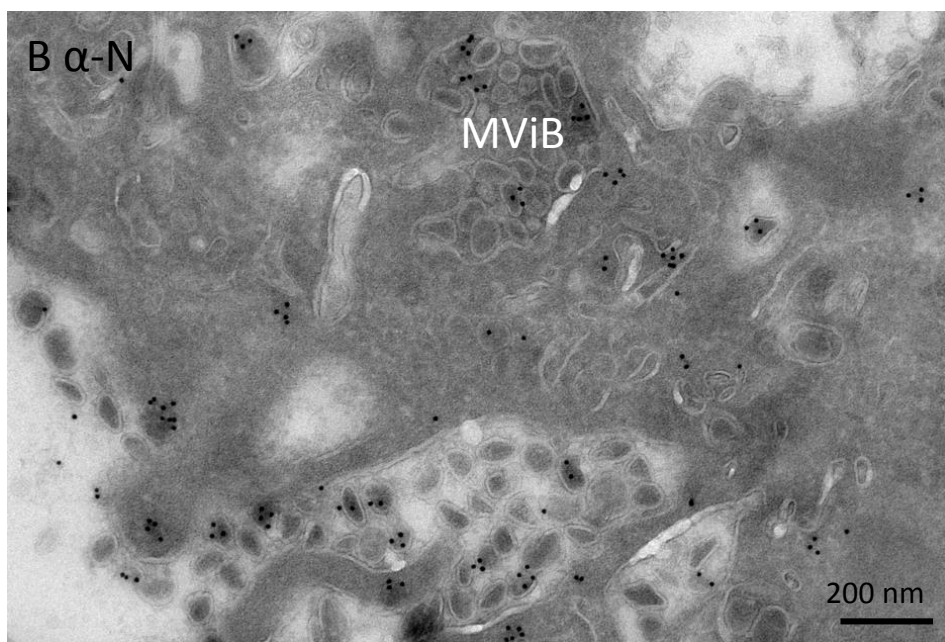
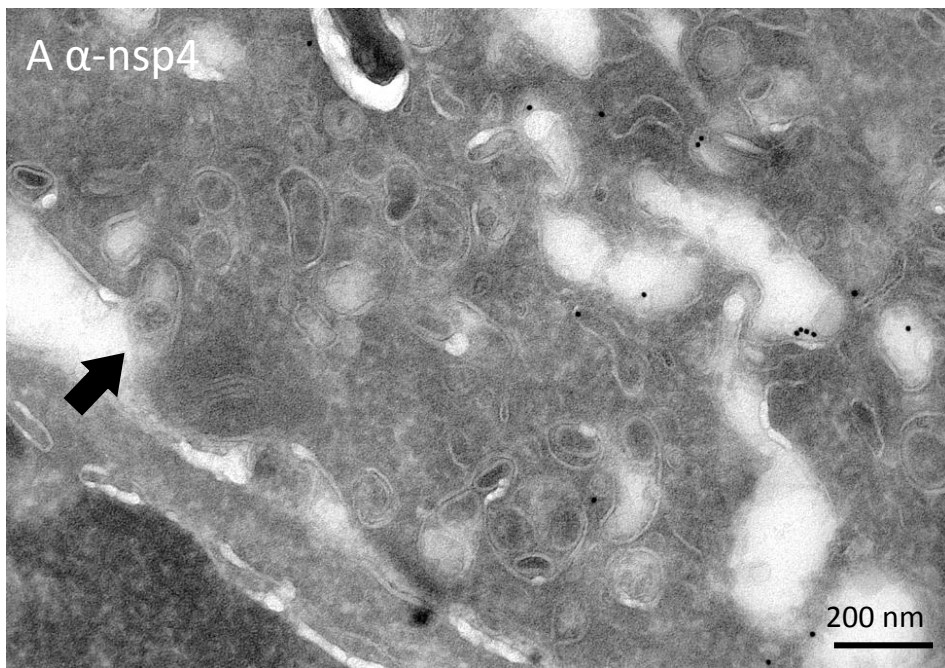




Figure 4

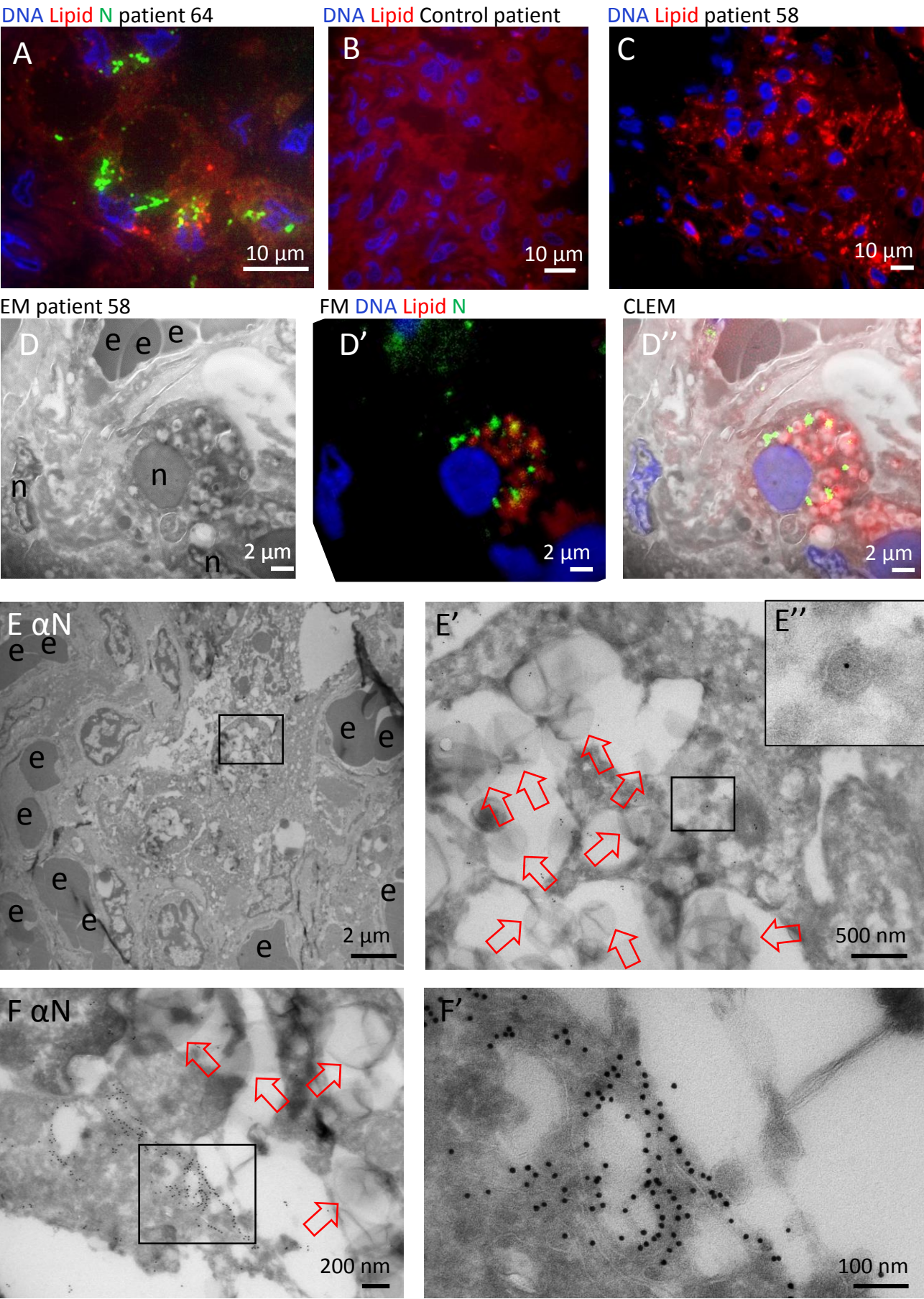




Figure 5

